A Vibratory Conveying Method for Planetary Regolith: Preliminary Experiment and Numerical Simulation

HUAZHI CHEN[1], **LIFANG LI**[2], **WEIWEI ZHANG**[1], **RONGKAI LIU**[1], **AND SHENGYUAN JIANG**[1]

[1]State Key Laboratory of Robotics and System, Harbin Institute of Technology, Harbin 150001, China
[2]Laboratory for Space Environment and Physical Sciences, Harbin Institute of Technology, Harbin 150001, China

Corresponding author: Shengyuan Jiang (jiangshy@hit.edu.cn)

ABSTRACT Planetary regolith conveying is an important process during planetary *in situ* resource utilization. After introducing finlike asperities on a longitudinally vibrated trough surface, we experimentally investigated the effects of vibration amplitude, frequency, and trough inclination angle on the particle flow state and directional conveying capacity. A numerical simulation based on the discrete element method (DEM) was then employed to study the detailed particle motion. Three flow states gradually appeared as the vibration strength increased: the particles remain stationary, flow down to the bottom of the trough, or directionally convey toward the discharge hole. The results indicated that the directional conveying capacity increased and decreased monotonically with increases in the vibration amplitude and trough inclination angle, respectively. The conveying capacity changed circuitously as the frequency increased and vanished when the frequency approached the resonant frequency of the trough. Additionally, according to the DEM simulation, breaking the force chains in the particle pile is necessary for conveying. The asymmetric force induced by the finlike asperities and its cumulative effect over time determines the particle flow state and conveying capacity. The particle flow velocity decreased as the granular layer height increased. This paper provides inspiration and guidance for designing a new type of conveyor for planetary regolith.
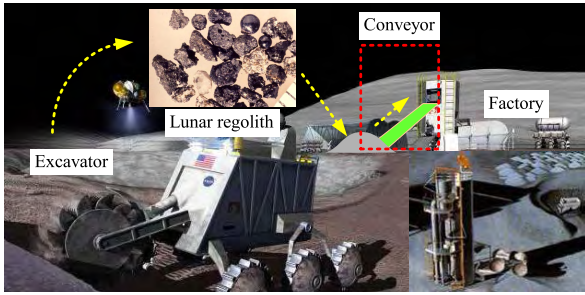
INDEX TERMS Planetary regolith, vibratory conveying, surface texture, particle flow, discrete element method.

I. INTRODUCTION

In situ resource utilization (ISRU) is an important basis for establishing a future planetary base (on the Moon or on Mars). ISRU involves using planetary regolith and rock as building materials, and metal and oxygen are manufactured from these raw materials [1]–[3]. In this process, conveyance is essential for raw materials, particularly granular materials (e.g., lunar regolith), as shown in Figure 1. In most cases, granular materials must be automatically and continuously transported from the ground to a certain height. Considering the constraints of lunar engineering, a vibratory conveyor with a simple configuration that consumes relatively little energy is more suitable than a belt conveyor [4]. Furthermore, a vibratory conveyor can transport high-temperature or corrosive materials because its trough can be readily made from a

refractory and corrosion-resistant material. These properties make such conveyors widely preferred in metallurgical and chemical industries. Great efforts have been made to extend vibratory conveyance theories and improve the performance of conveyors in engineering applications. Two types of vibratory conveyors are currently applied in practice and classified according to the direction of the vibration relative to the trough surface. The first type of vibratory conveyor features sinusoidal vibration acting obliquely on the trough [5]–[8], and the second type of vibratory conveyor features vibration parallel to the axis of the trough (i.e., the longitudinal direction) but with a nonsinusoidal profile [9], [10]. Materials cannot be directionally transported if the trough vibrates longitudinally with a sinusoidal waveform. However, such transport is enabled if the trough has an appropriate surface morphology (e.g., a sawtooth texture) [11]. This topic merits comprehensive study because of its potential value for improving the performance of current conveyors.

The associate editor coordinating the review of this manuscript and approving it for publication was Chaoyong Li.
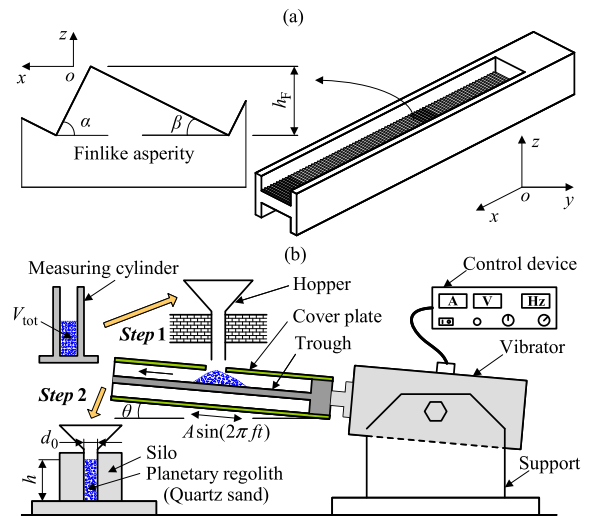
FIGURE 1. Concept of lunar regolith excavation and conveyance to establish a lunar base [2].

FIGURE 2. Experimental equipment: (a) sketch of the trough with finlike asperities; (b) sketch of the equipment.

Generally, granular materials are usually considered to be point masses for convenient theoretical analysis, but this simplification cannot reflect the actual properties of such materials. Previous research has established that granular materials exhibit complex properties under vibration, such as convection, heaping, size separation, and climbing in narrow channels [12]–[18]. A large amount of particle interaction causes the particle kinestate to be distinct from that of a single body on the vibratory conveyor. Moreover, the rugged surface intensifies the indeterminacy of the particle kinestate under vibration. In this case, the experiment becomes a convenient and effective way to investigate the apparent particle motion. However, the presence of a variety of multiple types of particles, particularly tiny and opaque particles, makes it challenging to experimentally study detailed particle motion in a trough. Therefore, the discrete element method (DEM) is a powerful way to study the particle behaviors of granular materials [19]–[24].

Most planetary regolith particles have small diameters. For example, the average diameters of lunar regolith particles are $0.07 \sim 0.13$ mm [25]. However, it is difficult to manufacture an asymmetric surface texture in a similar size to the small particles with ordinary processing techniques. Even if such a surface texture could be manufactured, it would be very expensive. Therefore, investigating the flow characteristics of planetary regolith on a longitudinally vibrated trough with a relatively large texture is more important. In this work, the selected texture is a series of finlike asperities. We report the effects of the vibration amplitude, frequency, and trough inclination angle on the granular material flow characteristics via a series of experiments. Then, we employ a DEM simulation to understand the detailed motion of the particles, which cannot be observed from the experiments. The results of this study are expected to be useful for designing a new type of conveyor for planetary regolith.

II. EXPERIMENTAL EQUIPMENT
Figure 2 shows a sketch of the experimental equipment. The trough was made from synthetic resin and had finlike asperities along an 80 mm (length) × 10 mm (width) surface [Figure 2(a)]. The height of each finlike asperity (h_F) was 0.4 mm. The tangent values of the major inclination angle (α)

and the lesser inclination angle (β) were 2.0 and 0.5, respectively. The planetary regolith was simulated with quartz sand that had a 0.1 mm average diameter ($0.09 \sim 0.106$ mm in fact) and a 2648 kg/m^3 real density.

As shown in Figure 2(b), the trough was fixed on a vibrator (HEV-50, manufactured by Foneng Technology and Industrial (Nanjing) Co., Ltd., Nanjing, China) whose amplitude (A) and frequency (f) can be adjusted by a control device. The sinusoidal vibration considered in this study can be expressed as

$$x = A \sin(2\pi f t) \tag{1}$$

The vibrator was mounted on a support, and the angle of its central axis relative to the horizon was θ. A silo with an inner diameter (d_0) of 5 mm was placed under the discharge hole to evaluate the quartz sand conveying capacity. In addition, a cover plate was attached to the trough to prevent the particles from slopping outside of the trough during vibration.

In this experiment, a certain volume of quartz sand (V_{tot}) was poured into a hopper and then heaped onto the middle of the trough surface with the finlike asperities. After initiating the vibrator, the trough vibrated along its central axis. The quartz sand that was transmitted toward the discharge hole of the trough ($+x$-direction in Figure 2) was collected by the silo. The collection process was recorded by a digital camera (SONY NEX-5C, the frame rate was 25 fps, i.e., the data were recorded every 0.04 s), where h is the heaping height [Figure 2(b)]. The quartz sand and the trough mass were sufficiently small that the bending of the trough caused by the weight of the granular material could be ignored.

III. EXPERIMENTAL RESULTS
A. PARTICLE FLOW ON THE VIBRATED TROUGH
The volume of the quartz sand poured into the hopper for each experiment was 550 mm^3 (determined by a measuring cylinder), and the inclination angle of the trough was set to 5°.

By adjusting the vibration parameters, we observed three flow states in the trough, as shown in Figure 3.

(a)

(b)

(c)

(d)
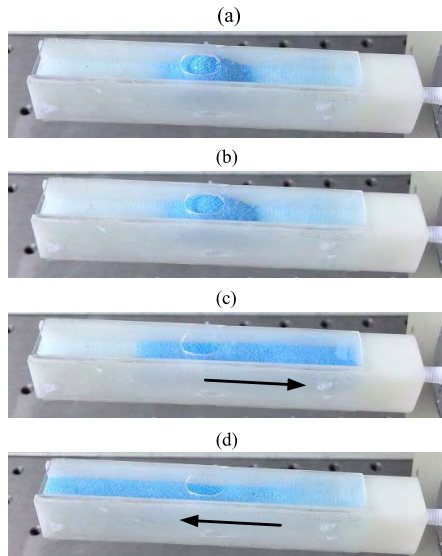
FIGURE 3. Particle states in the trough before and after vibration.
(a) Before vibration. **(b)** State 1: $A = 0.2$ mm, $f = 25$ Hz, and $\theta = 5°$.
(c) State 2: $A = 0.2$ mm, $f = 50$ Hz, and $\theta = 5°$. **(d)** State 3: $A = 0.2$ mm, $f = 70$ Hz, and $\theta = 5°$.

The particles in the trough were heaped in a conical shape before vibration, as shown in Figure 3(a). After a period of vibration, the particle heap had either retained this conical shape [Figure 3(b), State 1], flowed to the bottom of the trough [Figure 3(c), State 2], or moved to the discharge hole [Figure 3(d), State 3]. Generally, States 1 and 2 occurred with a weak vibration strength (Γ): $\Gamma = A \cdot (2\pi f)^2/g$, where g is the gravitational acceleration (g = 9.8 m/s^2).

To demonstrate the crucial role of the finlike asperities in conveying the particles, we arranged a comparison experiment by employing a smooth trough without any asperities; the results are shown in Figure 4. The particles flowed to the bottom of the smooth trough when the amplitude and frequency were 0.2 mm and 70 Hz (State 2), respectively, whereas the particles flowed to the discharge hole of the trough with finlike asperities under these conditions [Figure 3(d)].

Trough (no asperity)   **State 2** $A = 0.2$mm, $f = 70$Hz, $\theta = 5°$
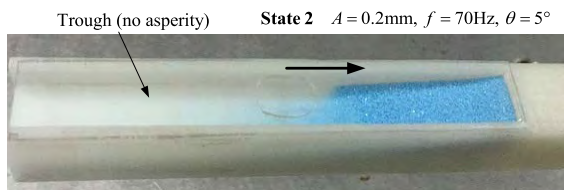
FIGURE 4. Particle flow state in the trough without finlike asperities.

Figure 5 shows the gathering process of the particles in the silo when the vibration frequency and amplitude were 50 Hz and 0.6 mm, respectively. The relationship between the time and heaping height is approximately linear. The slope shows

(a-1) 0 s   (a-2) 4 s   (a-3) 8 s   (a-4) 12 s   (a-5) 16 s

(b)
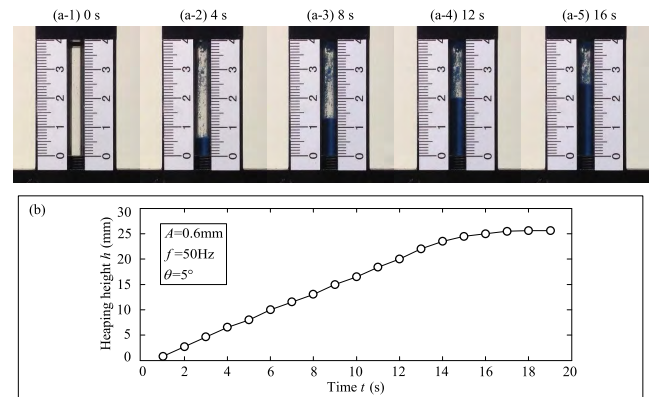
FIGURE 5. (a) Particle gathering process in silo; (b) relationship between heaping height and vibration time.

that the heaping velocity $v_{\mathrm{h}} = dh/dt$, which also reflects the particle conveying velocity. In this paper, we introduce the conveying rate (R_{c}) to evaluate the conveying capacity, which can be expressed as

$$R_c = \pi d_0^2 \cdot v_h / (4V_{tot}) \qquad (2)$$

The definition of the conveying rate represents the ratio of the conveying volume to the total volume per second. If $R_{\mathrm{c}} = 0$, no particles are collected in the silo.

Next, we studied the influence of A_{c}, f_{c}, and θ on R_{c}. The results are presented in the following section. The operational parameters in each case are listed in Table 1.

TABLE 1. Operational parameters in the experiments.

No.	Amplitude [mm]	Frequency [Hz]	Inclination angle [°]
1	0.1–1.0 (step: 0.1)	50	5
2	0.6	10–80 (step: 5)	5
3	0.1–1.0 (step: 0.1)	10–80 (step: 5)	5
4	0.6	50	1–10 (step: 1)

B. EFFECT OF THE AMPLITUDE ON CONVEYING

Figure 6 shows the relationship between the conveying rate and amplitude (No. 1) at a frequency of 50 Hz and a trough inclination angle of 5° . When the amplitude was less than $A_{\mathrm{c}} = 0.3$ mm ($\Gamma = 3$), the particles remained in the trough throughout the experiment. When the amplitude was greater than 0.3 mm, the particles were delivered to the silo. This shows that the particles require sufficient vibration strength to escape from the oblique trough.

The conveying rate increases as the amplitude increases. Larger amplitude leads to a larger asymmetric displacement in each vibration period, and this effect enhances the conveying velocity of the particles in the trough.

C. EFFECT OF THE FREQUENCY ON CONVEYING

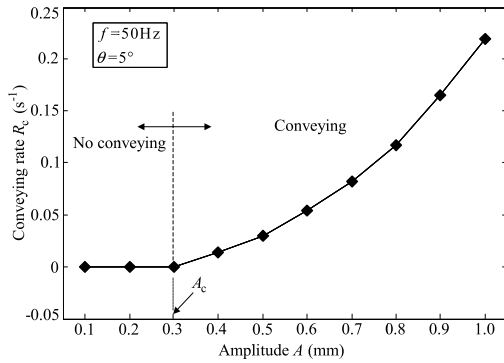The relationship between the conveying rate and the frequency (No. 2) when the amplitude and inclination angle are

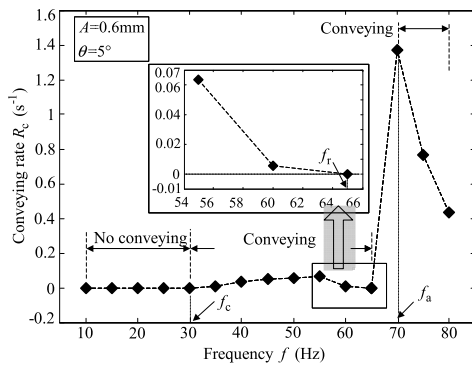**FIGURE 6.** Relationship between the conveying rate and amplitude.

FIGURE 7. Relationship between the conveying rate and frequency.
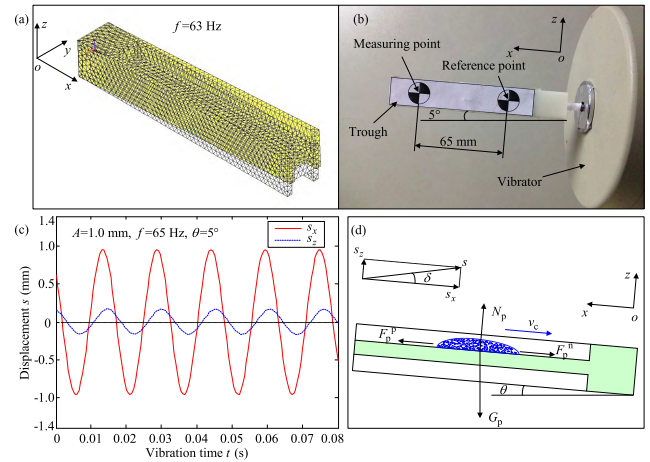

FIGURE 8. Trough vibration state under a frequency of 65 Hz: (a) first mode shape in the FEM simulation; (b) measuring point and reference point for the high-speed camera in the experiment; (c) measuring point displacement components in the x- and z-directions; (d) trough resultant vibration and particle mechanical model.

displacement components in the x-direction and z-direction, normal contact force, particle gravity, and friction force in the $+x$-direction and $-x$-direction, respectively). This case is similar to the movement of material on an ordinary vibratory conveyor [5]. Certainly, the particles flowed to the bottom of the trough according to this mechanism.

The conveying rates obtained for different combinations of amplitude and frequency (No. 3) are shown in Figure 9. In view of the obvious differences in the conveying rate values, we divided the results into two parts, with 65 Hz as the boundary. The results again indicated that the conveying rate increased monotonically with amplitude, but varied circuitously with frequency.
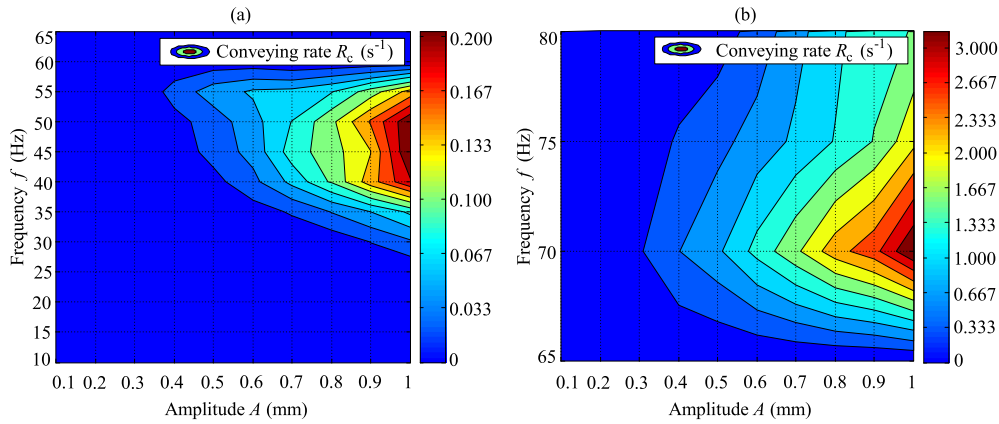
The result indicated that the same Γ may not correspond to the same R_c. For example, Γ was 3.9 when $A = 0.8$ mm and $f = 35$ Hz and when $A = 0.2$ mm and $f = 70$ Hz; however, for these cases, R_c was 0.042 and 0.072, respectively. Thus, when studying this kind of conveying, A and f should both be stated, rather than being combined as Γ.
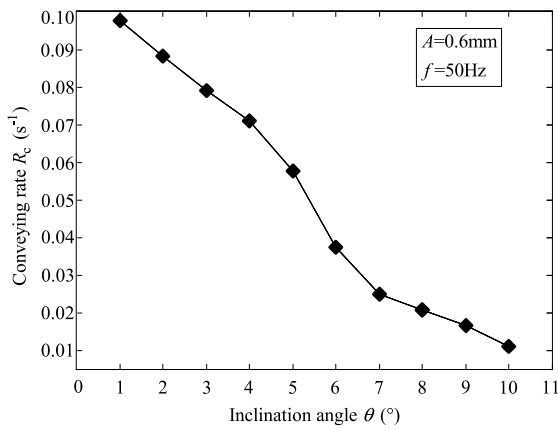
D. EFFECT OF THE INCLINATION ANGLE ON CONVEYING

By adjusting the trough inclination angle from 1–10° (No. 4), we achieved different conveying rates, as shown in Figure 10. Obviously, the conveying rate decreased as the inclination angle increased, which indicates that the particles flowed more slowly at larger inclination angles at a given amplitude and frequency. It can be seen that the gravitational component along the $-x$-direction played an important role in decreasing R_c.

IV. DEM SIMULATION AND ANALYSIS

The experimental results indicated that granular materials could be directionally conveyed on a vibrated trough with finlike asperities under appropriate vibration conditions. The flow states varied according to the amplitude, frequency, and trough inclination angle. In particular, the influence of the

kept at 0.6 mm and 5°, respectively, is shown in Figure 7. The particles could not be delivered to the silo when the frequency was less than $f_c = 30$ Hz ($\Gamma = 2.2$), whereas the directional conveyance was obvious as the frequency increased above 30 Hz. However, the relationship between the conveying rate and frequency was not monotonic. Instead, the conveying rate decreased after the frequency exceeded 70 Hz (f_a).

An interesting phenomenon is that the conveying rate decreased to zero when the frequency approached $f_r = 65$ Hz. In fact, the particles slid down to the bottom of the trough (State 2) at this frequency.

We speculated that the flow mechanism changed at 65 Hz. Therefore, we analyzed a model of the trough based on the finite element method (FEM, the package was ANSYS 14.0, where the material parameters of the trough were the same as listed in Table 3 and the mesh size was set to 2 mm). The first- and second-order resonant frequencies were found to be 63 Hz and 454 Hz, respectively. The singular frequency of 65 Hz is close to the first-order resonant frequency, and the mode shape is shown in Figure 8(a). This indicates that the trough also vibrates along the z-direction, which was verified experimentally [Figure 8(b) and (c); the data were recorded by a high-speed camera (Phantom V12, manufactured by Vision Research Inc., USA, and the frame rate was set to 2000 fps.)]. The resultant vibration was oblique and the included angle δ was approximately 11° , as shown in Figure 8(d) (where s_x, s_z, N_p, G_p, F_p^p, F_p^n denote the

FIGURE 9. Contour plot showing the conveying rate as a function of amplitude and frequency: (a) below 65 Hz; (b) above 65 Hz.

FIGURE 10. Relationship between the conveying rate and trough inclination angle.

frequency was more complicated than the influences of the other two parameters. To understand the details of the particle motion, we employed a DEM simulation. In this way, a preliminary explanation about the different phenomena could be given.

In this study, the preliminary DEM simulation was used to reveal the particle behaviors on the vibratory trough, without attempting to generate simulation data that are exactly the same as the experimental data. Therefore, the process of the contact parameters verification and particle shape were simplified.

A. DEM MODEL DESCRIPTION
In our simulation, a three-dimensional DEM based on the soft-sphere model [26]–[28] was used. Each particle exhibited two types of movement, translational motion and rotational motion, as governed by Newton's second law:

$$\begin{cases} m_i \frac{d\boldsymbol{v}_i}{dt} = m_i \boldsymbol{g} + \sum_{j=1}^{n_i} \boldsymbol{F}_{ij} \\ I_i \frac{d\boldsymbol{\omega}_i}{dt} = \sum_{j=1}^{n_i} \boldsymbol{T}_{ij} \end{cases} \qquad (3)$$

where $\boldsymbol{v}_i$ and $\boldsymbol{\omega}_i$ are the translational and angular velocity vectors of particle i, respectively; m_i and I_i are the mass and rotational inertia of particle i, respectively; $\boldsymbol{g}$ is the gravitational acceleration; n_i is the number of particles (including the trough wall if possible) j in collision with particle i; and $\boldsymbol{F}_{ij}$ and $\boldsymbol{T}_{ij}$ are the contact force and torque generated between particles i and j, respectively, which are composed of several components, namely,

$$\begin{cases} \boldsymbol{F}_{ij} = \boldsymbol{F}_{n,ij} + \boldsymbol{F}_{t,ij} \\ \boldsymbol{T}_{ij} = \boldsymbol{T}_{t,ij} + \boldsymbol{T}_{r} \end{cases} \qquad (4)$$

where $\boldsymbol{F}_{n,ij}$ and $\boldsymbol{F}_{t,ij}$ are the normal and the tangential forces, respectively; $\boldsymbol{T}_{t,ij}$ is the torque caused by the tangential force; and $\boldsymbol{T}_{r}$ is the rolling resistance when relative rotation occurs between the contacting particles. This rolling resistance is due to the elastic deformation of the surfaces caused by rolling.

Due to the absence of cohesive forces, electrostatic forces and heat transfer, the Hertz-Mindlin contact model was appropriate to calculate $\boldsymbol{F}_{n,ij}$ and $\boldsymbol{F}_{t,ij}$. The rolling resistance $\boldsymbol{T}_{r}$ is related to the normal force. Then the contact forces and torques that include particle-particle and particle-wall interactions are as follows [29]–[35]:

The parameters μ_{s} and μ_{r} are the static friction and rolling resistance coefficients, respectively; $\delta_{n,ij}$ and $\delta_{t,ij}$ are the normal overlap and tangential displacements, respectively; $\boldsymbol{v}_{n,ij}$ and $\boldsymbol{v}_{t,ij}$ are the relative normal and tangential velocities, respectively; $\boldsymbol{n}_{ij}$ is the unit vector pointing from the center of particle i to object j (particle or trough wall); ω_{ni} is the unit angular velocity vector at the contact point when relative rotation occurs, which is consistent with the direction of rotation and used to determine the rolling resistance direction; E^*, G^*, R^* and m^* are the equivalent Young's modulus, shear modulus, curvature radius and mass, respectively, which are related to Young's moduli, shear moduli, curvature radii and masses of the two objects in contact with each other; and e is the restitution coefficient.

Based on the model and the matched calculation procedure, the particle's kinestate in each time step is obtained. In this

TABLE 2. Force and torque equations used in the contact model.

Item	Equation	No.
Normal force	$F_{n,ij} = \left(-\dfrac{4}{3} E^* \sqrt{R^*} \left(\delta_{n,ij} \right)^3 - 2\sqrt{\dfrac{5}{6}} \beta_c \sqrt{S_n m^*} \left\| v_{n,ij} \right\| \right) n_{ij}$	(5)
Tangential force	$F_{t,ij} = \begin{cases} -F_{te,ij}^n - 2\sqrt{\dfrac{5}{6}} \beta_c \sqrt{S_t m^*} \, v_{t,ij} & \text{for } \left\|F_{t,ij}\right\| \le \mu_s \left\|F_{n,ij}\right\| \\ -\mu_s \left\|F_{n,ij}\right\| v_{t,ij}/\left\|v_{t,ij}\right\| & \text{for } \left\|F_{t,ij}\right\| > \mu_s \left\|F_{n,ij}\right\| \end{cases}$	(6a)
	$F_{te,ij}^n = F_{te,ij}^{n-1} + S_t^n \Delta\delta_{t,ij} \qquad \text{for } \Delta F_{n,ij} \ge 0$	(6b)
	$F_{te,ij}^n = F_{te,ij}^{n-1}\left(\dfrac{S_t^n}{S_t^{n-1}}\right) + S_t^n \Delta\delta_{t,ij} \quad \text{for } \Delta F_{n,ij} < 0$	(6c)
Torque	$\begin{cases} T_{t,ij} = R_i n_{ij} \times F_{t,ij} \\ T_r = -\mu_r \left\|F_{n,ij}\right\| R_i \omega_{ni} \end{cases}$	(7)
	$\begin{cases} S_n = 2E^*\sqrt{R^*\delta_{n,ij}} \\ S_t = 8G^*\sqrt{R^*\delta_{n,ij}} \\ \beta_c = \dfrac{\ln e}{\sqrt{\ln^2 e + \pi^2}} \end{cases}$	(8)
Coefficient	$\begin{cases} \dfrac{1}{E^*} = \dfrac{1-v_i^2}{E_i} + \dfrac{1-v_j^2}{E_j} \\ \dfrac{1}{G^*} = \dfrac{1-v_i}{G_i} + \dfrac{1-v_j}{G_j} \\ \dfrac{1}{R^*} = \dfrac{1}{R_i} + \dfrac{1}{R_j} \\ \dfrac{1}{m^*} = \dfrac{1}{m_i} + \dfrac{1}{m_j} \end{cases}$	(9)

TABLE 3. DEM simulation parameters.

Parameter	Symbol	Value
Particle:		
Particle diameter [mm]	d_p	0.1
Particle solid density [kg/m³]	ρ_p	2648
Shear modulus [Pa]	G_p	5×10^7
Poisson's ratio	v_p	0.3
Particle–particle restitution coefficient	$e_{p\text{-}p}$	0.6
Particle–particle static friction coefficient	$\mu_{s,p\text{-}p}$	0.6
Particle–particle rolling resistance coefficient	$\mu_{r,p\text{-}p}$	0.075
Trough:		
Density [kg/m³]	ρ_w	1070
Shear modulus [Pa]	G_w	8.63×10^8
Poisson's ratio	v_w	0.39
Particle–trough restitution coefficient	$e_{p\text{-}w}$	0.6
Particle–trough static friction coefficient	$\mu_{s,p\text{-}w}$	0.6
Particle–trough rolling resistance coefficient	$\mu_{r,p\text{-}w}$	0.075

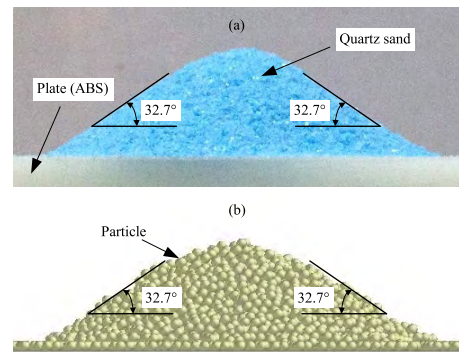**FIGURE 11.** Repose angle in experiment (a) and simulation (b).

work, the EDEM 2.6 software package (DEM Solutions Ltd., Edinburgh, UK) was employed for the numerical simulation. However, before calculation, the conditions should be set in detail, particularly the micro contact parameters e, μ_s and μ_r, as described in the following section.

B. SIMULATION CONDITIONS

An assembly of 1,500 spherical particles was considered in this simulation. Due to the small deviation in the size of the quartz sand and to shorten the calculation time, the particles in the simulation had a fixed diameter of 0.1 mm and a solid density of 2648 kg/m³. The sizes of the trough and the finlike asperities were the same as in the experiment. The Hertz-Mindlin (no-slip) model integrated in EDEM was employed for the particle–particle and particle–trough interactions. The other conditions are listed in Table 3. The material parameters of the quartz sand and trough were obtained from the suppliers of the raw materials. The shear modulus of particle was set to 5×10^7 Pa to improve the computational efficiency. A simple and common method to determine the contact parameters is matching the repose angles obtained in the experiments and simulations [36], [37]. In this study, the parameters were validated with this method, as shown in Figure 11. Although the conveying capacity in the simulation based on the parameters validated by this method may be different from that in the experiment under the same vibration conditions, the three flow states (phenomena) were the same.

From this perspective, the parameters validated by matching repose angles can be accepted in the simulation.

Prior to the onset of vibration, the particles were generated and heaped in the middle of the trough. After being stably heaped, the trough vibrated along the x-direction. The vibration time t was 4 s, and the data were recorded every 0.001 s. Considering the amount and accuracy of the simulation results, the Rayleigh time step Δt_R was employed as a reference in EDEM, which can be expressed as

$$\Delta t_R = \frac{\pi d_p}{2\left(0.163v_p + 0.877\right)}\sqrt{\frac{\rho_p}{G_p}} \tag{10}$$

Generally, the actual time step used in EDEM was $0.05 \sim 0.4 \, \Delta t_R$, and then we set the time step to $0.25 \, \Delta t_R$ (i.e., 3.1×10^{-7} s) since we found that the simulation result at a smaller value ($0.05 \, \Delta t_R$) was the same as that at $0.25 \, \Delta t_R$. In addition, the trough inclination angle θ was $5°$.

C. SIMULATION RESULTS AND ANALYSIS

Figure 12 shows that the particles remained stationary and maintained their accumulated state (State 1) under low-
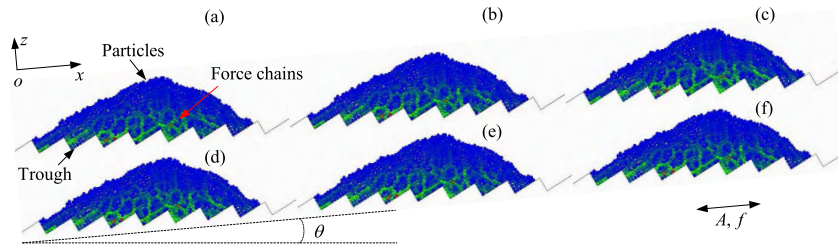
FIGURE 12. Distributions of the force chains in a vibration period T (State 1): A = 0.02 mm and f = 40 Hz. (a) Before vibration. (b) $t = t_0$. (c) $t = t_0 + 0.25T$. (d) $t = t_0 + 0.5T$. (e) $t = t_0 + 0.75T$. (f) $t = t_0 + T$.
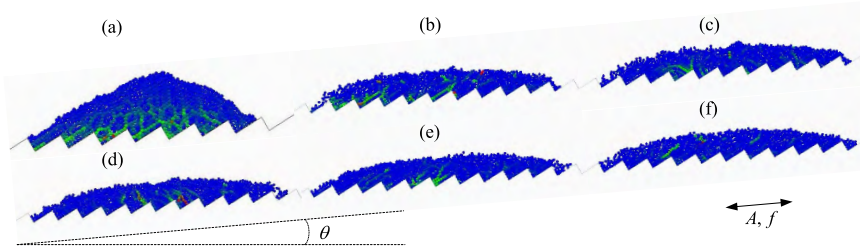
FIGURE 13. Distributions of the force chains in a vibration period T while particles flow: A = 0.2 mm and f = 40 Hz. (a) Before vibration. (b) $t = t_0$. (c) $t = t_0 + 0.25T$. (d) $t = t_0 + 0.5T$. (e) $t = t_0 + 0.75T$. (f) $t = t_0 + T$.

intensity vibration. In this simulation, the amplitude and frequency were 0.02 mm and 40 Hz, respectively.

The contact forces among the accumulated particles were not uniform, and the contact forces among some particles were much greater than others. The configurations of these force paths were similar to interlaced chains, as shown in Figure 12(a). Then, the force chains acted as a skeleton to support the whole particle pile.

The force chains can resist strong pressure but slight shear force. In this simulation, the vibrated trough provided an alternating shear force on the particle pile, but the shear force was too weak to break the force chains in this condition ($A = 0.02$ mm and $f = 40$ Hz). Thus, the particle pile maintained its initial shape throughout the vibration [Figure 12(b) $\sim$ (f)]. When the vibration intensity was increased, the force chains were destroyed, and the particles started flowing, as shown in Figure 13.

By adjusting the amplitude, the particles flowed toward the bottom of the trough (State 2) when $A = 0.2$ mm and toward the discharge hole (State 3) when $A = 0.4$ mm, as shown in Figure 14(a) and (b). We analyzed the detailed evolution of the particle flow velocity v_{PAR} together with the trough vibration velocity v_{TRO} to understand the mechanism of the two states.
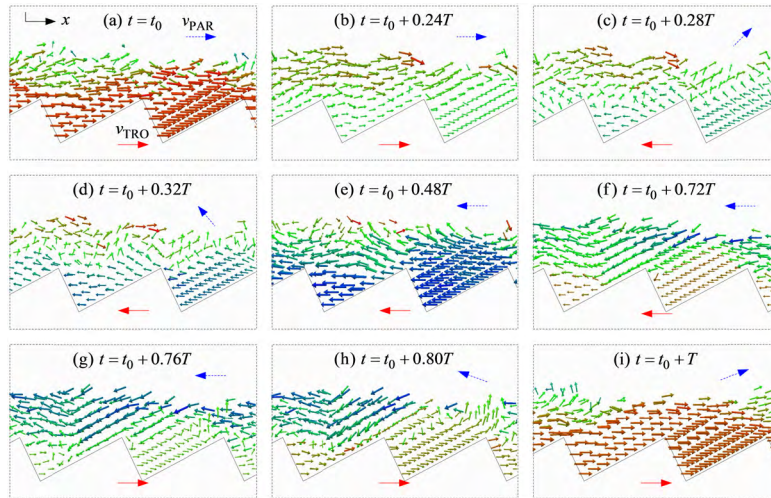
Rotating the viewport 5° (θ) clockwise, the evolution of the particle flow velocity vector in a vibration period is shown in Figure 15, where $A = 0.2$ mm and $f = 40$ Hz. The arrows indicate the movement direction, and the colors indicate the velocity magnitude. Blue, green and red represent the minimum, middle and maximum magnitudes, respectively.
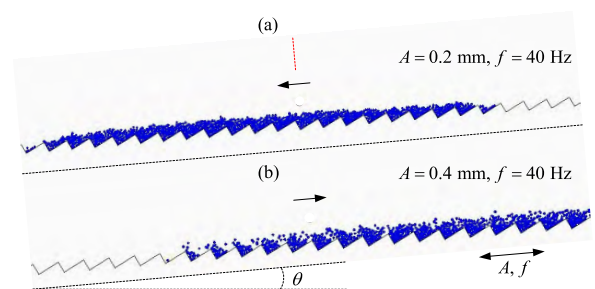

FIGURE 14. Particle flow states in the simulation: (a) State 2; (b) State 3.

At t_0, the trough moved toward the $+x$ direction with a maximum velocity [Figure 15(a)], and the particles also flowed toward the same direction. After one quarter of the period, the trough moved toward the $-x$ direction and the particles changed their flow direction in a short time, as shown in Figure 15(c) and (d). After three quarters of the period, the trough moved toward the $+x$ direction again, but the particles did not immediately flow together with the trough, as shown in Figure 15(g) and (h); the particles spent more time changing the flow direction from $-x$ to $+x$ than the opposite situation. In this way, we macroscopically observed that the particles flowed toward the $-x$ direction (State 2) as the time increased.

Figure 16 shows the particle motion after the amplitude was increased to 0.4 mm. One quarter of the period later, the trough and the particles between two adjacent asperities turned to the $-x$ direction, but the particles above the asperities did not. The particles above the asperities kept flowing toward the $+x$ direction and slid over the top of

FIGURE 15. Evolution of particle flow velocity vector in a vibration period T, A = 0.2 mm and f = 40 Hz.
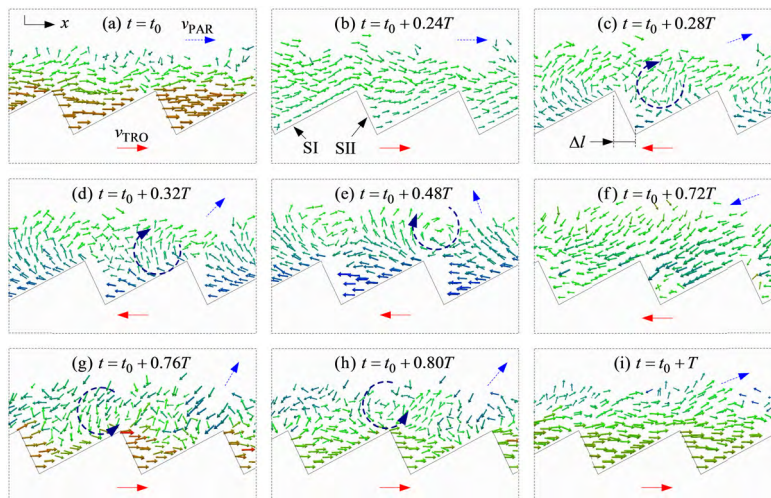
FIGURE 16. Evolution of the particle flow velocity vector in a vibration period T: A = 0.4 mm and f = 40 Hz.

the gentle slope (SI). Then, these particles flowed forward a distance Δl relative to the trough, and then flowed toward $+x$ and $-x$ directions and formed a clockwise convection circle. The convection circle moved upward and finally disappeared until all of the particles flowed toward the $-x$ direction, as shown in Figure 16(c) $\sim$ (f). After three quarters of the period, the trough once again moved toward the $+x$ direction. The particles between two adjacent asperities struck the abrupt slope (SII) and immediately move together with the trough. Then, these particles collided with the upper particles, and an anticlockwise convection circle appeared. In the intense collision, the upper particles quickly turned to the opposite direction, as shown in Figure 16(g) and (h). Therefore, we macroscopically observed that the particles flowed toward the $+x$ direction (State 3) as the time increased.

Forces can alter the kinestate of an object according to Newton's laws of motion. The average component force acting on the particles in the x-direction (F_{px}) is shown in Figure 17(a). The finlike asperities ensured that the positive force was larger than the negative force in both cases. However, the particle kinestate is not only dependent on the force F_{px} but also the vibration time t. These factors affect the component velocity (v_p) in the x-direction as follows:

$$v_p(t) = \frac{1}{m_p} \cdot \int_0^t F_{px}(t) \cdot dt \qquad (11)$$

where m_p is the average particle mass. The relationship between the velocity v_p and vibration time t is shown in Figure 17(b). The summation of the areas surrounded by the curve and the horizontal line reflects the conveying (offset) displacement of the particles. The conveying
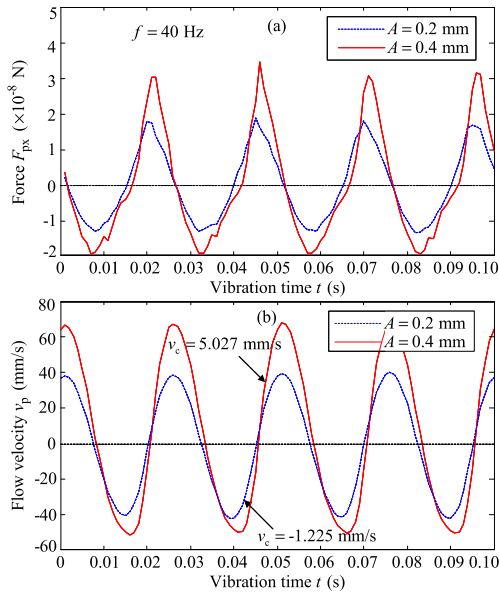
FIGURE 17. Particle component force in the x-direction (a) and flow velocity (b) in States 2 and 3.

velocity (v_c) can be obtained as

$$v_c = \frac{1}{T} \cdot \int_t^{t+T} v_p(t) \cdot dt \tag{12}$$

Compared with v_p, v_c is more intuitive for describing the results because it simultaneously reflects the flow direction (by the sign "+" or "−") and magnitude (by the absolute value). In this simulation, $v_c = -1.225$ mm/s and 5.027 mm/s for $A = 0.2$ mm and 0.4 mm, respectively. Furthermore, as v_c can be expediently obtained from the simulation, it was employed instead of R_c to evaluate the conveying capacity in the DEM simulation.

We also observed the differences in v_p across different particle layers. We divided the particles into three layers, as shown in Figure 18(a). The values of v_p in the three layers are
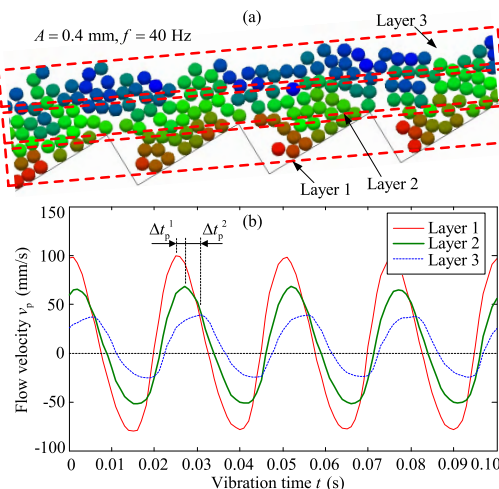

FIGURE 18. Particle flow velocity distribution (a) and magnitude (b) in different layers: A = 0.4 mm and f = 40 Hz.

shown in Figure 18(b). The results indicate that v_p decreased and exhibited a slight lag (Δt_p^i, $i = 1, 2$) in higher layers. The reason is that the underlying particles were in direct contact with the trough and obtained kinetic energy under vibration. As the particles contacted each other, the upper layer particles gradually flowed under the driving of the underlying particles, which led to a time difference in the particle motion for the different layers. In this process, the kinetic energies of the upper layer particles were smaller than those of the underlying particles due to the energy losses caused by the collisions between the particles. Correspondingly, the velocities of the upper layer particles were smaller than those of the underlying particles. In short, this phenomenon implies that the vibration energy is dissipated when transmitted among the particles.

V. CONCLUSION

For the purpose of planetary regolith conveying, a type of vibratory conveying method that considers finlike asperities on a trough surface was introduced. In this study, the effects of vibration amplitude, frequency, and trough inclination angle on the granular material flow state and conveying capacity were experimentally studied. A numerical simulation based on DEM was employed to identify the mechanism of the observed phenomena, and the following conclusions were drawn.

1) As the vibration intensity increased, the simulated planetary regolith exhibited three flow states in the trough: the particles remain stationary (State 1), flow to the bottom of the trough (State 2), or move to the discharge hole (State 3).

2) In the experiment, the conveying capacity monotonically increased with increasing amplitude A but monotonically decreased with increasing trough inclination angle θ. The conveying capacity also increased with frequency f when f_c (30 Hz) $< f \leq f_a$ (70 Hz) but decreased when $f > f_a$. As f approached the resonant frequency of the trough (65 Hz), the particles moved into State 2 because of the transformation in the trough's response at this frequency.

3) According to the DEM simulation, breaking the force chains in the particle pile is necessary for conveying. The asymmetric force induced by the finlike asperities and its cumulative effect over time determine the particle flow state and conveying capacity. Moreover, the flow velocity v_p decreases as the granular layer height increases.

This study provides inspiration and guidance for designing a new type of conveyor for planetary regolith. In future works, we will focus on the effects of particle size and shape on conveying capacity.

ACKNOWLEDGMENT

REFERENCES

[1] R. Mueller and I. Townsend, "Lunar regolith simulant feed system for a hydrogen reduction reactor system," in *Proc. 47th AIAA Aerosp. Sci. Meeting*, Orlando, FL, USA, Jan. 2009, p. 1658.

[2] G. Sanders, W. Larson, and K. Sacksteder, "NASA lunar mining and construction activities and plans," Canadian Institute of Mining Conference and Exhibition, Toronto, Canada, Tech. Rep. JSC-CN-18219, 2009. [Online]. Available: https://ntrs.nasa.gov/archive/nasa/casi.ntrs.nasa.gov/20090020653.pdf

[3] S. Jiang *et al.*, "Technical schemes of investigation and *in-situ* utilization for lunar surface generalized resources," *J. Deep Space Explor.*, vol. 2, no. 4, pp. 291–301, 2015.

[4] Y. Zhao, F. Huang, and Z. Zhao, "Dynamic analysis on vertical vibratory conveyor," *Adv. Mater. Res.*, vols. 694–697, pp. 3–6, May 2013.

[5] E. M. Sloot and N. P. Kruyt, "Theoretical and experimental study of the transport of granular materials by inclined vibratory conveyors," *Powder Technol.*, vol. 87, no. 3, pp. 203–210, Jun. 1996.

[6] G. H. Lim, "On the conveying velocity of a vibratory feeder," *Comput. Struct.*, vol. 62, no. 1, pp. 197–203, Jan. 1997.

[7] J. V. Vilán, A. S. Robleda, P. J. G. Nieto, and C. C. Placer, "Approximation to the dynamics of transported parts in a vibratory bowl feeder," *Mechanism Mach. Theory*, vol. 44, no. 12, pp. 2217–2235, Dec. 2009.

[8] X. Kong, X. Zhang, Q. Li, and B. Wen, "Dynamical analysis of vibratory feeder and feeding parts considering interactions by an improved increment harmonic balance method," *Proc. Inst. Mech. Eng., C, J. Mech. Eng. Sci.*, vol. 229, no. 6, pp. 1029–1040, Jun. 2015.

[9] D. Reznik and J. Canny, "The coulomb pump: A novel parts feeding method using a horizontally-vibrating surface," in *Proc. IEEE Int. Conf. Robot. Automat. (ICRA)*, vol. 1, May 1998, pp. 869–874.

[10] B. Guo, Z. Duan, J. Zheng, and Y. He, "Analysis of material movement of non-harmonic horizontally vibrated conveyer," *Chin. J. Mech. Eng.*, vol. 48, no. 1, pp. 104–110, Jan. 2012.

[11] A. Mitani, T. Yoshimura, and S. Hirai, "Feeding of submillimeter-sized microparts along a saw-tooth surface using only horizontal vibration: Analysis of convexities on the surface of microparts," in *Proc. IEEE Int. Conf. Automat. Sci. Eng. (CASE)*, Sep. 2007, pp. 69–76.

[12] E. Clément, J. Duran, and J. Rajchenbach, "Experimental study of heaping in a two-dimensional 'sand pile'," *Phys. Rev. Lett.*, vol. 69, no. 8, pp. 1189–1194, Aug. 1992.

[13] J. A. C. Gallas, H. J. Herrmann, and S. Sokołowski, "Convection cells in vibrating granular media," *Phys. Rev. Lett.*, vol. 69, no. 9, pp. 1371–1374, Aug. 1992.

[14] J. B. Knight, H. M. Jaeger, and S. R. Nagel, "Vibration-induced size separation in granular media: The convection connection," *Phys. Rev. Lett.*, vol. 70, no. 24, pp. 3728–3731, Jun. 1993.

[15] K. Liffman, G. Metcalfe, and P. Cleary, "Granular convection and transport due to horizontal shaking," *Phys. Rev. Lett.*, vol. 79, no. 23, pp. 4574–4576, Dec. 1997.

[16] D. A. Huerta and J. C. Ruiz-Suárez, "Vibration-induced granular segregation: A phenomenon driven by three mechanisms," *Phys. Rev. Lett.*, vol. 92, no. 11, Mar. 2004, Art. no. 114301.

[17] M. E. Möbius, X. Cheng, P. Eshuis, G. S. Karczmar, S. R. Nagel, and H. M. Jaeger, "Effect of air on granular size separation in a vibrated granular bed," *Phys. Rev. E, Stat. Phys. Plasmas Fluids Relat. Interdiscip. Top.*, vol. 72, no. 1, Jul. 2005, Art. no. 011304.

[18] C. Liu, F. Zhang, P. Wu, and L. Wang, "Effect of hoisting tube shape on particle climbing," *Powder Technol.*, vol. 259, pp. 137–143, Jun. 2014.

[19] P. A. Cundall and O. D. L. Strack, "A discrete numerical model for granular assemblies," *Géotechnique*, vol. 79, no. 1, pp. 47–65, Mar. 1979.

[20] E. Simsek, S. Wirtz, V. Scherer, H. Kruggel-Emden, R. Grochowski, and P. Walzel, "An experimental and numerical study of transversal dispersion of granular material on a vibrating conveyor," *Particulate Sci. Technol.*, vol. 26, no. 2, pp. 177–196, Mar. 2008.

[21] Y. Shimizu, "Three-dimensional DEM simulation of conveying granular materials by horizontal screw," in *Proc. Discrete Element Methods, Numer. Modeling Discontinua*, pp. 415–422, 2002.

[22] Y. Han, F. Jia, Y. Zeng, L. Jiang, Y. Zhang, and B. Cao, "DEM study of particle conveying in a feed screw section of vertical rice mill," *Powder Technol.*, vol. 311, pp. 213–225, Apr. 2017.

[23] Y. Xu, J. Musser, T. Li, J. T. Padding, and W. A. Rogers, "Particles climbing along a vertically vibrating tube: Numerical simulation using the discrete element method (DEM)," *Powder Technol.*, vol. 320, pp. 304–312, Oct. 2017.

[24] F. Zhou, S. Hu, Y. Liu, C. Liu, and T. Xia, "CFD-DEM simulation of the pneumatic conveying of fine particles through a horizontal slit," *Particuology*, vol. 16, pp. 196–205, Oct. 2014.

[25] V. Gromov, "Physical and mechanical properties of lunar and planetary soils," *Earth, Moon, Planets*, vol. 80, nos. 1–3, pp. 51–72, Dec. 1998.

[26] N. Mitarai and H. Nakanishi, "Hard-sphere limit of soft-sphere model for granular materials: Stiffness dependence of steady granular flow," *Phys. Rev. E, Stat. Phys. Plasmas Fluids Relat. Interdiscip. Top.*, vol. 67, no. 2, Feb. 2003, Art. no. 021301.

[27] A. B. Stevens and C. M. Hrenya, "Comparison of soft-sphere models to measurements of collision properties during normal impacts," *Powder Technol.*, vol. 154, nos. 2–3, pp. 99–109, Jul. 2005.

[28] S. R. Schwartz, D. C. Richardson, and P. Michel, "An implementation of the soft-sphere discrete element method in a high-performance parallel gravity tree-code," *Granular Matter*, vol. 14, no. 3, pp. 363–380, May 2012.

[29] Y. Zeng, F. Jia, Y. Zhang, X. Meng, Y. Han, and H. Wang, "DEM study to determine the relationship between particle velocity fluctuations and contact force disappearance," *Powder Technol.*, vol. 313, pp. 112–121, May 2017.

[30] K. L. Johnson, K. Kendall, and A. D. Roberts, "Surface energy and the contact of elastic solids," *Proc. Roy. Soc. A, Math. Phys. Sci.*, vol. 324, no. 1558, pp. 301–313, Sep. 1971.

[31] R. D. Mindlin and H. Deresiewicz, "Elastic spheres in contact under varying oblique forces," *Trans. ASME, J. Appl. Mech.*, vol. 20, no. 8, pp. 327–344, 1953.

[32] B. Ren *et al.*, "CFD-DEM simulation of spouting of corn-shaped particles," *Particuology*, vol. 10, no. 5, pp. 562–572, Oct. 2012.

[33] C. Thornton, S. J. Cummins, and P. W. Cleary, "An investigation of the comparative behaviour of alternative contact force models during inelastic collisions," *Powder Technol.*, vol. 233, pp. 30–46, Jan. 2013.

[34] Y. C. Zhou, B. D. Wright, R. Y. Yang, B. H. Xu, and A. B. Yu, "Rolling friction in the dynamic simulation of sandpile formation," *Phys. A, Stat. Mech. Appl.*, vol. 269, nos. 2–4, pp. 536–553, Jul. 1999.

[35] J. Ai, J.-F. Chen, J. M. Rotter, and J. M. Rotter, "Assessment of rolling resistance models in discrete element simulations," *Powder Technol.*, vol. 206, no. 3, pp. 269–282, Jan. 2011.

[36] S. M. Derakhshani, D. L. Schott, and G. Lodewijks, "Micro–macro properties of quartz sand: Experimental investigation and DEM simulation," *Powder Technol.*, vol. 269, pp. 127–138, Jan. 2015.

[37] C. J. Coetzee and D. N. J. Els, "Calibration of granular material parameters for DEM modelling and numerical verification by blade–granular material interaction," *J. Terramech.*, vol. 46, no. 1, pp. 15–26, Feb. 2009.

HUAZHI CHEN received the B.S. and M.S. degrees in mechanical engineering from the Harbin Institute of Technology, China, in 2012 and 2014, respectively, where he is currently pursuing the Ph.D. degree with the School of Mechatronics Engineering. His research interests include planetary drilling and sampling, and planetary exploration robot systems.

LIFANG LI received the B.S. degree from Yanshan University, Hebei, China, in 2003, and the M.S. and Ph.D. degrees from the Harbin Institute of Technology, Harbin, China, in 2007 and 2012, respectively, where she is currently an Associate Professor with the Laboratory for Space Environment and Physical Sciences. Her current research interest includes mechanism optimal design.

WEIWEI ZHANG received the B.S. degree in mechanical engineering from Beihua University, Jilin, China, in 2012, and the M.S. degree in mechanical engineering from the Harbin Institute of Technology, Harbin, China, in 2014, where he is currently pursuing the Ph.D. degree with the School of Mechatronics Engineering. His research interests include planetary drilling and sampling, and planetary exploration robot systems.

SHENGYUAN JIANG received the B.S. degree in mechanical metallurgy from the North China University of Technology, Beijing, China, in 1992, and the M.S. and Ph.D. degrees in mechanical design and theory from the School of Mechatronics Engineering, Harbin Institute of Technology, Harbin, China, in 1998 and 2001, respectively, where he has been a Professor with the Department of Manufacturing Engineering for Aviation and Aerospace, since 2011. His current research interests include planetary penetration, drilling, and sampling techniques, aerospace system design, optimization, and simulation.

• • •

RONGKAI LIU received the B.S. degree in mechanical engineering from Dalian Maritime University, Dalian, China, in 2017. He is currently pursuing the M.S. degree with the School of Mechatronics Engineering, Harbin Institute of Technology. His research interests include planetary penetrating, investigating, and sampling, and planetary exploration robot systems.